analytical chemistry

Article

pubs.acs.org/ac

Biomolecular Steric Hindrance Effects Are Enhanced on Nanostructured Microelectrodes

Sahar Sadat Mahshid,[†] Alexis Vallée-Bélisle,[‡] and Shana O. Kelley*[,†]

[†]Department of Pharmaceutical Science, Leslie Dan Faculty of Pharmacy, University of Toronto, Toronto, Ontario M5S 3M2 Canada
[‡]Département de Chimie, Université de Montréal, Montréal, Québec H3T 1J4 Canada

Supporting Information

ABSTRACT: The availability of rapid approaches for quantitative detection of biomarkers would drastically impact global health by enabling decentralized disease diagnosis anywhere that patient care is administered. A promising new approach, the electrochemical steric hindrance hybridization assay (eSHHA) has been introduced for quantitative detection of large proteins (e.g., antibodies) with a low nanomolar detection limit within 10 min. Here, we report the use of a nanostructured microelectrode (NME) platform for eSHHA that improves the performance of this approach by increasing the efficiency and kinetics of DNA hybridization. We demonstrated that eSHHA on nanostructured microelectrodes leverages three effects: (1) steric hindrance effects at the nanoscale, (2) a size-dependent hybridization rate of DNA complexes, and (3) electrode morphology-dependent blocking effects. As a proof of concept, we showed that the sensitivity of eSHHA toward a model antibody is enhanced using NMEs as scaffolds for this reaction. We improved the detection limit of eSHHA, taking advantage of nanostructured surfaces to allow the use of longer capture strands for detection of proteins. Finally, we concluded that using the eSHHA approach in conjunction with nanostructured microelectrodes is an advantageous alternative to conventional macroelectrodes as the sensitivity and detection limits are enhanced.

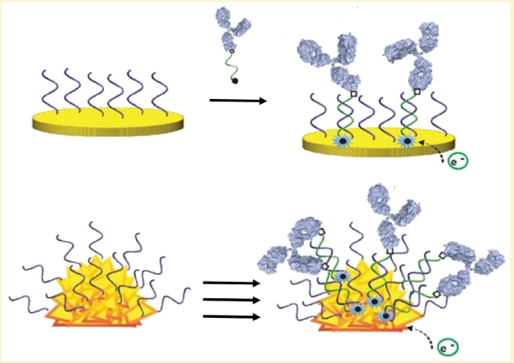

Over the past two decades, high-performance detection of biomarkers has advanced with the development of qualitative and quantitative optical, mass-based, or electrochemical assays. Electrochemical sensors are promising as they can be optimized to be rapid, reagentless, and easily multiplexed.[1−3] Using direct electronic signal readout, high sensitivities can be achieved along with ease of calibration and the use of inexpensive signal transduction equipment.[4,5] As well, high levels of selectivity can be achieved through the use of surface-immobilized monolayers of biological receptors that are compatible with real samples.[6−15] Electrochemical biomolecular sensors are therefore in principle promising for low-cost clinical diagnostics, as they require no laboratory infrastructure and can be adapted for rapid time-to-result molecular testing.[16]

However, realizing high levels of sensitivity and specificity in electrochemical sensing strategies can be challenging. Nanomaterials can impact the sensitivity of electrochemical biosensing approaches by improving the efficiency of probe-target complexation and the kinetics of electrochemical reactions.[5,17−20] Optimization of the surface morphology of nanostructured electrodes leads to signal amplification and significant improvement of detection limits, in part by offering sensors with large surface-to-volume ratios that can be formatted in high-density sensing arrays.[21] Metallic nanostructures such as nanoparticles and ordered arrays of nanowires have been deposited on the sensing electrodes because of their large electroactive surface area and enhanced electronic properties.[21−23] Many other types of nanomaterials have been shown to enhance performance,[24,25] demonstrating the general utility of this approach.

Recent efforts to develop chip-based sensors based on electrodeposited metals produced a new class of three-dimensional microelectrodes.[21,26−30] These nanostructured microelectrodes (NMEs) exhibit attomolar detection limits for DNA and RNA analytes. With high surface-to-volume ratios, these structures bearing controllable surface morphologies can selectively amplify signal transduction. A number of recent electrochemical assays for detection of DNAs, RNAs, and proteins have been developed using NMEs as a sensing platform.[5,27,29,31−35] Hierarchical nanostructured microelectrodes consisting of a gold core structure decorated with palladium nanoparticles are particularly effective. The gold core structures enable microelectrodes up to 100 μm to be fabricated leading to large surface areas, while Pd nanoparticles enhance the binding affinities of the surface-immobilized probe molecules.[31]

Here, we report the use of nanostructured microelectrodes (NME) in combination with a new type of biomolecular detection assay that relies on steric effects at the sensor surface

Received: April 30, 2017
Accepted: August 22, 2017
Published: August 22, 2017

DOI: 10.1021/acs.analchem.7b01595
Anal. Chem. 2017, 89, 9751−9757

to detect proteins and antibodies. The electrochemical steric hindrance hybridization assay, eSHHA, is a versatile DNA-based detection approach that uses steric hindrance caused by different types of biomolecular targets to inhibit DNA−DNA hybridization at the electrode surface.[36] NMEs are electrodes with unique surface morphologies that we hypothesized could enhance the performance of this sensing strategy. By using the eSHHA with this type of sensing electrode, we have improved its efficiency and demonstrated the advantages of using three-dimensional electrodes for biomolecular detection.

MATERIALS AND METHODS

DNA Sequences. The complete materials list appears in the Supporting Information. DNA strands used in this manuscript were HPLC purified and synthesized by Biosearch Technologies Inc. (Novato, CA). The sequences of the strands used in this work are shown in Table 1.

Table 1. Sequences of Signaling and Capture DNA Strands

capture strands	
5′-HS-(CH2)6- AAGG AAA GGG AAG AAG	
5′-HS-(CH2)6-GGAA TGA AGT CGA TGG ACCT TAC CTG CCT TGT	
signaling strands	
Dig.	5′-Digoxigenin-CTT CTT CCC TTT CCTT-MB
Ctrl.	5′-CTT CTT CCC TTT CCTT-MB
biotin	5′-Biotin-ACA AGG CAG GTA AGGT CCA TCG ACT TCA TTCC -MB

Macroelectrode Preparation. Detailed sensor fabrication procedures can be found in literature references.[36,37] Briefly, polycrystalline gold disk electrodes (2 mm diameter; BAS, West Lafayette, IN) were prepared by electrochemical cleaning (a series of oxidation and reduction cycling in 0.5 M H_2SO_4, 0.01 M KCl/0.1 M H_2SO_4, and 0.05 M H_2SO_4[36]) and the area was estimated based on the geometry of the electrode: 0.03 cm^2.

Nanostructured Microelectrode Preparation. Chip substrates (fabrication procedure in Supporting Information) were rinsed with acetone, isopropyl alcohol, and DI water, respectively, and dried with nitrogen flow. They each have seven apertures with the gold layer at the bottom (Figure 1A). Electrodeposition of three-dimensional (3D) NMEs were done in a three-electrode configuration cell, having the 10 μm-aperture on the chip as working electrode, a platinum wire as counter electrode and a Ag/AgCl reference electrode, at room temperature. The chip was first placed in a solution containing 50 mM $HAuCl_4$ and 0.5 M HCl, having the connectors outside the solution to prevent the short-circuit (Figure 1B). DC potentiostatic amperometry at 0 mV (for spiky structures) and −550 (for flaky structures) was applied for 100 s to deposit the microelectrodes of two different morphology (Figure 1C). Following the washing with DI water and drying with air blow, the chip was transferred to 5 mM H_2PdCl_4 and 0.5 M $HClO_4$ solution for electrodeposition of nanoparticles of Pd at −250 mV for 10 s to induce the surface nanoroughness. After it was washed with DI water and dried with blowing air, the chip electroplated with NMEs was ready for DNA (capturing strands) immobilization. Area of the NMEs was calculated 0.005 mm^2 as was described in Supporting Information.

Functionalization of Macroelectrodes (MacroE)/NMEs. Capturing DNA strands (0.1 mM) were incubated with TCEP, Tris(2-carboxyethyl) phosphine hydrochloride, (10 mM) for 1 h to allow reduction of disulfide bonds. This solution was diluted to desired concentrations in PBS. Macroelectrodes were incubated in 150 μL solution of capturing strands overnight. Electrodes were then rinsed with DI water, and incubated in 150 μL of 3 mM MCH, 6-mercapto-1-hexanol, in buffer for another 3 h to displace nonspecifically adsorbed DNA and passivate the remaining electrode area. After thoroughly rinsing with DI water, electrodes were stored in PBS. To functionalize NMEs, 50 μL of capturing strand solution was put on the chip, to cover all over the area of NME and kept overnight. After washing with PBS, 50 μL of 3 mM MCH was put on the chip for 3 h and finally washed thoroughly with PBS. The capturing strand surface density calculation is described in Supporting Information.

Calculation of Hybridization Kinetics. The rate of DNA−DNA hybridization on the surface is estimated by the modified first-order Langmuir equation,[38]

$$I(t) = I_{max}(1 - e^{-kt})$$

where $I(t)$ and I_{max} are the current values at time t and maximum number of hybridization, respectively, and k is the concentration-dependent rate constant (equal to $k_{eff}C_0$, where

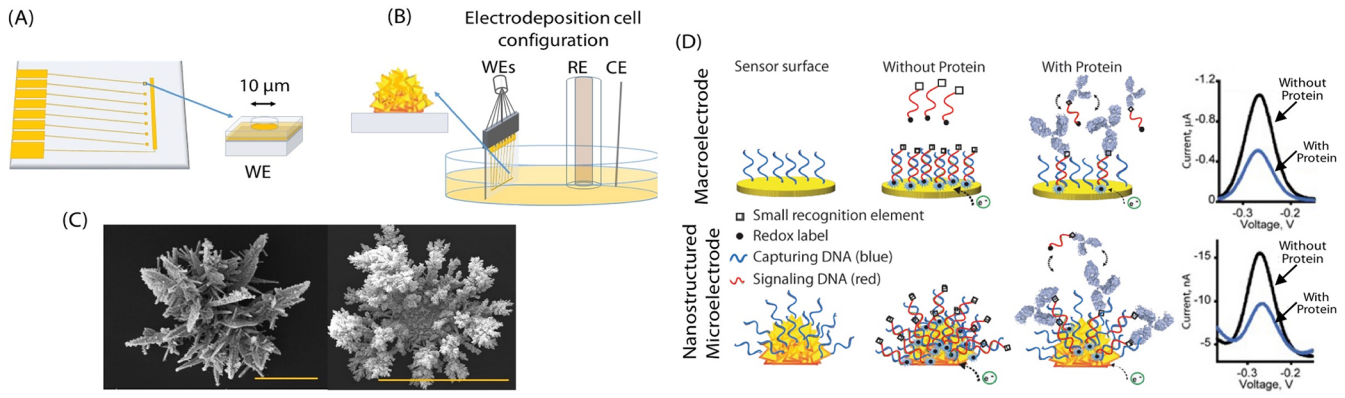

Figure 1. Investigation of eSHHA performance using the nanostructured microelectrode (NME) platform. (A) Schematic illustration of a glass substrate with microscale apertures that serve as templates for NME electroplating. (B) The growth of NMEs in a three-electrode electrochemical cell. (C) SEM images of NMEs with spiky (left) and flaky (right) structures (yellow scale bars are 20 μm). (D) Schematic illustration of eSHHA on the macroelectrode (top) and the NME (bottom), with a starting configuration of capturing strands on the electrode surface (left), upon binding to the signaling strands without and with (middle and left) target protein. Representative electrochemical signals are shown for each electrode type.

DOI: 10.1021/acs.analchem.7b01595
Anal. Chem. 2017, 89, 9751−9757

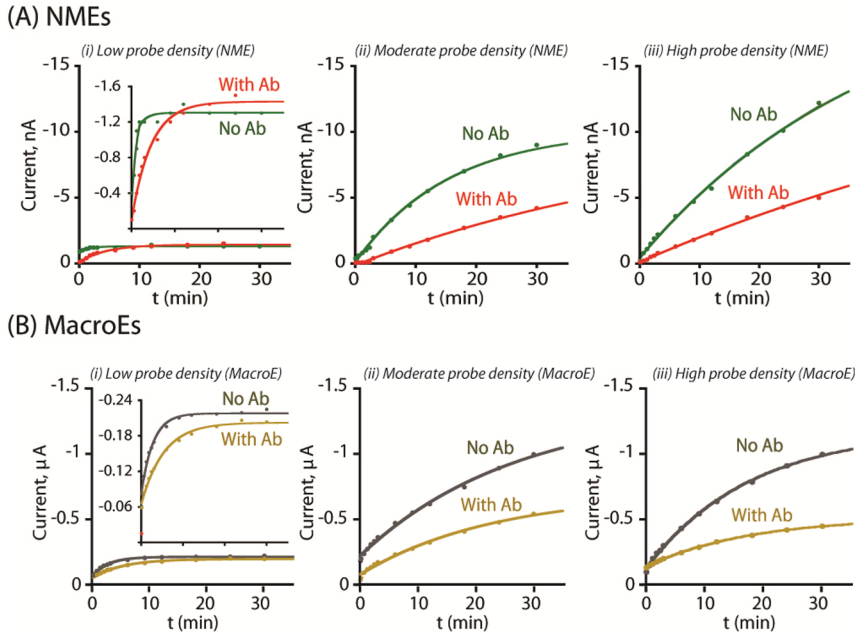

Figure 2. Kinetics of hybridization for (A) NMEs and (B) MacroEs, functionalized with low (30 nM, left), moderate (100 nM, middle), and high (3000 nM, right) densities of capturing strands. Measurements were performed with free DNA targets (no Ab) and with complexed antibody (with Ab).

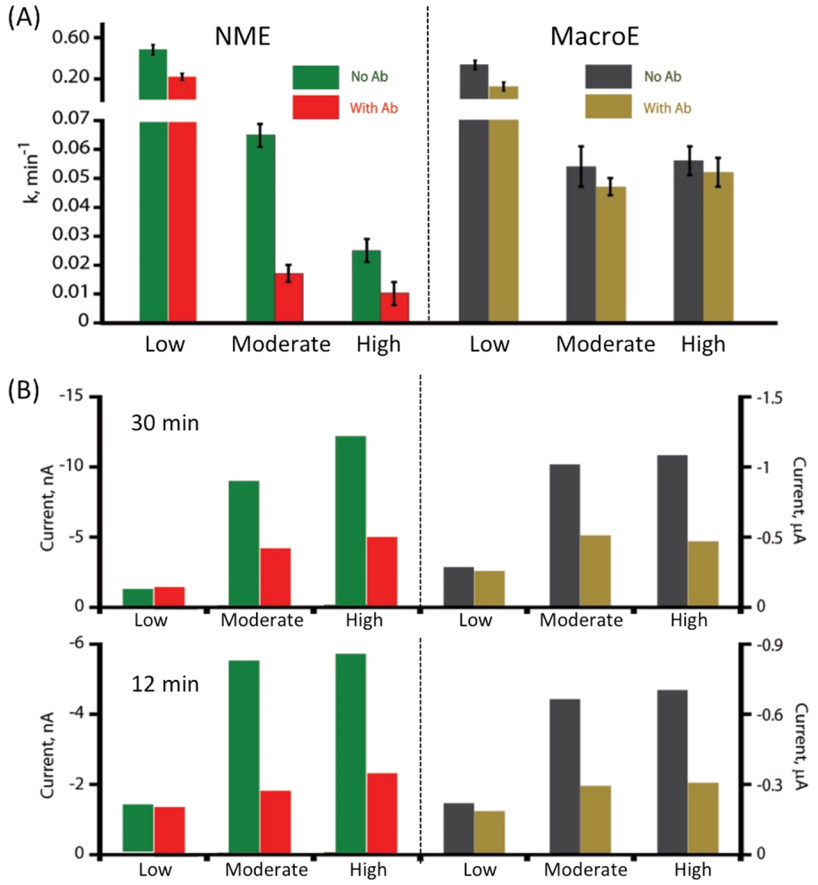

Figure 3. Comparison of (A) hybridization rate and (B) current levels after 12 and 30 min on the surface of NMEs and MacroEs functionalized with low (30 nM, left), moderate (100 nM, middle), and high (3000 nM, right) capturing strand concentrations. Measurements were collected in the presence and absence of antibody.

k_{eff} is the effective rate constant (M^{-1} s^{-1}), and C_0 is concentration of residual strands equal to the concentration of target DNA). We assumed a perfect electron transfer that only takes place upon hybridization of DNA strand to the

DOI: 10.1021/acs.analchem.7b01595
Anal. Chem. 2017, 89, 9751−9757

Table 2. Hybridization Kinetics for NMEs and MacroEs with Low (30 nM), Moderate (100 nM), and High (3 μM) Densities

	NMEs					
	low		moderate		high	
	k (min^{-1})	$t_{1/2}$ (min)	k (min^{-1})	$t_{1/2}$ (min)	k (min^{-1})	$t_{1/2}$ (min)
no Ab	0.56 ± 0.06	2 ± 1	0.065 ± 0.004	10 ± 1	0.025 ± 0.004	28 ± 5
with Ab	0.220 ± 0.035	3 ± 2	0.017 ± 0.003	41 ± 4	0.010 ± 0.004	67 ± 7
	MacroEs					
	low		moderate		high	
	k (min^{-1})	$t_{1/2}$ (min)	k (min^{-1})	$t_{1/2}$ (min)	k (min^{-1})	$t_{1/2}$ (min)
no Ab	0.35 ± 0.045	2 ± 1	0.054 ± 0.007	13 ± 1	0.056 ± 0.005	12 ± 1
with Ab	0.19 ± 0.04	4 ± 4	0.047 ± 0.003	15 ± 1	0.052 ± 0.005	13 ± 2

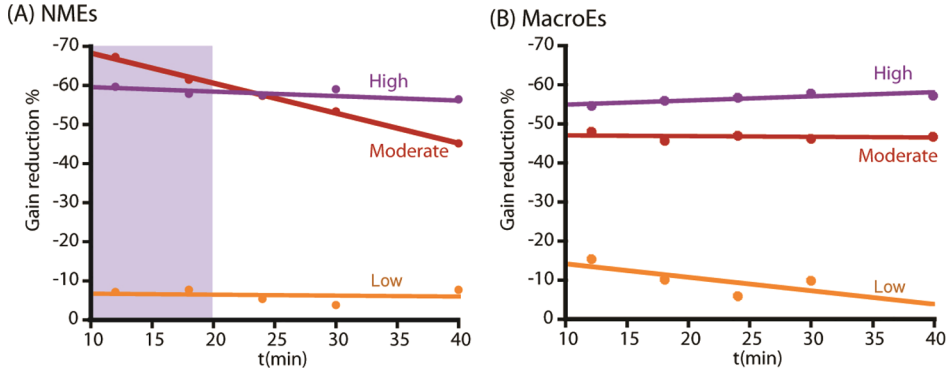

Figure 4. Time dependence of gain reduction upon detection of antibody on (A) NMEs and (B) MacroEs functionalized with low, moderate, and high density of capturing strands.

surface. Current at time t, $I(t)$, represents the number of successful hybridization events at the surface at time t. The corresponding half-time for hybridization, $t_{1/2}$, is then[39]

$$t_{1/2} = \frac{\ln(2)}{k}$$

Electrochemical Measurements. Electrochemical measurements were performed at room temperature using two workstations BASi EC Epsilon potentiostat and EmStat MUX potentiostat multiplexer (Palmsens Instruments, Netherland) in a standard three-electrode cell containing a platinum counter electrode (Sigma-Aldrich) and a Ag/AgCl (3 M NaCl) reference electrode (CHI). Experimental data were collected using square wave voltammetry (SWV) from −0.05 to −0.45 V in increments of 0.001 V vs. Ag/AgCl, with an amplitude of 50 mV and a frequency of 60 Hz. Peak currents were fit using the manual fit mode in the BASi software in case of measurements in Epsilon workstation and PStrace software in case of measurements in Palmsens workstation.

All measurements were taken immediately after adding 100 nM of the signaling strands to the sample containing the target proteins (i.e., no preincubation is needed). Results are presented in terms of current (knowing that the geometric area of the electrode is 0.03 cm^2 on macroelectrodes and 0.005 mm^2 on NMEs).

Gain Reduction. Gain represents difference in peak currents obtained before and after target addition divided by initial peak current.

Error Bars. Each experiment has at least seven replicates as there exists seven NMEs on each chip for each immobilization and target solution. Error bars represent standard error.

RESULTS AND DISCUSSION

Assessing the Performance of a Steric Hindrance Assay Using Nanostructured Electrodes. eSHHA relies on steric effects that are harnessed to hinder DNA−DNA hybridization on the surface of an electrode (Figure 1D) to detect target proteins. A signaling strand is designed that features two conjugated molecules: (1) a redox-active label, methylene blue (MB), and (2) a recognition element specific to the protein of interest (here, digoxigenin for the antidigoxigenin antibody or biotin for streptavidin). Depending on the size of target molecule (e.g., antibody or protein) attached to the recognition element on the signaling DNA strand, steric effects alter the efficiency of hybridization for the immobilized DNA capture strands.[36] In the absence of target molecules, the signaling DNA strands hybridize to the densely packed layer of capture strands on the surface, generating an electrochemical signal because the redox label is localized on the surface. However, in the presence of target proteins that attach to the recognition element on the signaling DNA strands, fewer copies can approach the electrode surface because of steric hindrance and the signal is decreased.

The larger the size or the higher the concentration of target molecule, the bigger the steric hindrance effect, and the more that a target molecule will suppress DNA hybridization. We hypothesized that 3D nanostructured microelectrodes (NMEs) might dramatically affect the surface hybridization characteristics and thus the steric hindrance assay performance.

Effect of Nanostructured Electrodes on Assay Kinetics. eSHHA requires high DNA densities on the surface of an electrode to promote the steric hindrance effect. We measured surface densities of the capture DNA probes used in eSHHA and observed a dramatic difference in the levels of DNA surface density that can be achieved with macroelectrodes

DOI: 10.1021/acs.analchem.7b01595
Anal. Chem. 2017, 89, 9751−9757

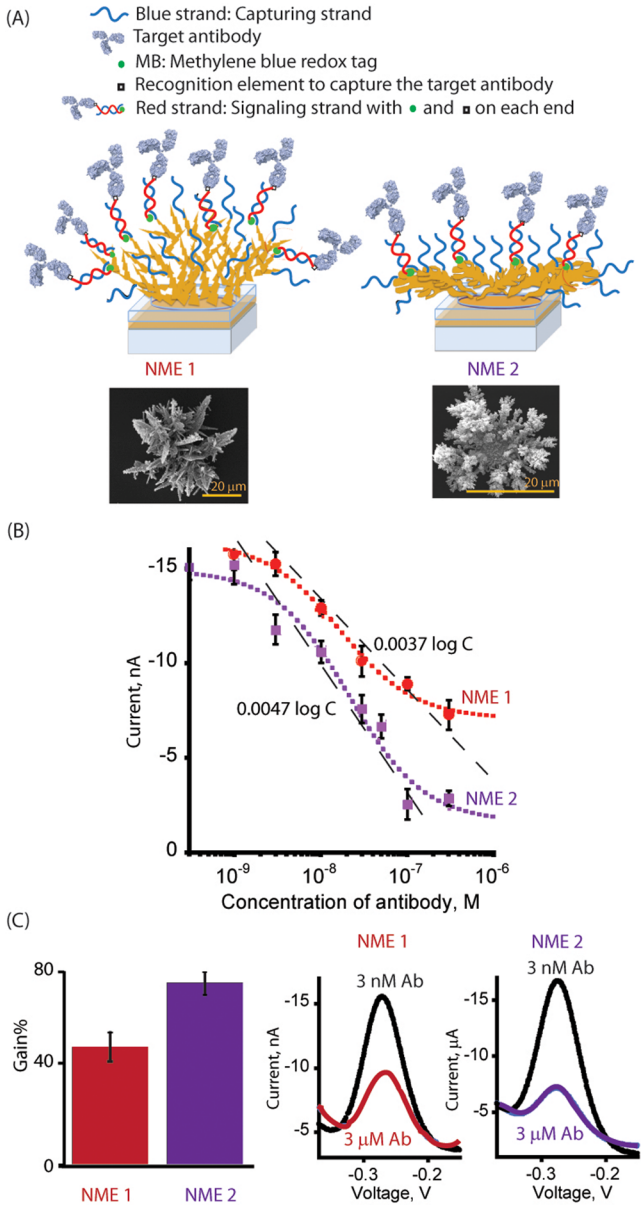

Figure 5. (A) Comparison of eSHHA performance on NMEs with two different morphologies generated using two different electrodeposition potentials. (B) Comparison of the sensitivity of eSHHA on different NMEs. (C) Comparison of the signal reduction on the two different NME structures by measuring the gain reduction observed upon antibody introduction. The SWV curves on NME1 and NME2 show the current difference between 3 nM and 3 μM antibody. Scale bar is 20 μm.

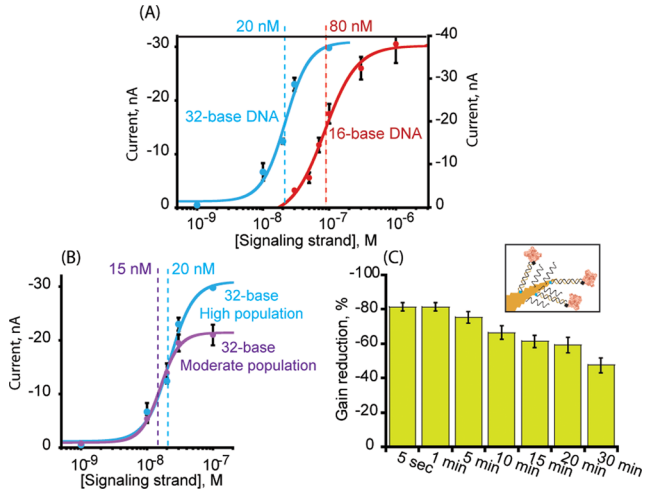

Figure 6. Improvement of gain and detection sensitivity with longer capture strands. (A) Dose−response curves collected using NMEs and increasing concentration of a 16-base (red curve) and a 32-base (blue curve) signaling strand. (B) Comparison of the dose−response curves with increasing concentration of 32-base signaling strand on high (blue) and moderate (purple) NMEs. (C) Gain reduction achieved using 10 nM streptavidin.

and NMEs. While surface coverages plateau at ~1 × 10^{12} molecules/cm^2 for macroelectrodes, surface coverages were 10-fold higher for the NMEs (Figure S1). This difference likely relates to the curvature of the surfaces of NMEs that allows probe molecules to realize higher packing levels because of the deflection angles created by highly curved surfaces.[40]

The differential hybridization efficiencies and kinetics were then compared for the two types of electrodes to explore whether there was a difference that could be exploited to enhance the performance of eSHHA (Figure 2). Free DNA targets, as well as those carrying complexed antibodies, were hybridized with immobilized capture strands. As reported previously, we found that eSHHA requires moderate or high surface coverages in order for steric hindrance effect to take place.[36] However, the kinetics of hybridization of the DNA on the macroelectrodes exhibited little changes in presence or absence of complexed antibodies at all of the surface coverages (Figure 3A, right). In contrast, the hybridization kinetics on the NMEs were significantly suppressed in the presence of the tethered antibody for moderate and high surface coverages (most pronounced for the moderate densities of capture probes) (Figure 3A, left).

eSHHA performed using NMEs relies not only on the overall efficiency of the binding of a complexed signaling strand to an electrode but also on the change in kinetics of hybridization. The data presented in Figure 3 highlight this point. On macroelectrodes, eSHHA does not exhibit large differences in signal kinetics for the free versus antibody-complexed signaling DNA. The lower current levels reached in the presence of antibodies is therefore solely attributable to the fact that fewer signaling DNA hybridize on the surface of the electrode. In contrast, the kinetics of hybridization in the presence of antibodies is significantly reduced on NMEs (4-fold). This results in larger gain values being achieved relative to the macroelectrodes at shorter incubation times (Table 2).

The time dependence of the gain confirms that only the NMEs produce signals that are modulated by the kinetics of hybridization (Figure 4). The maximal gain for the assay when performed using NMEs is achieved at early time points (e.g., 10 min) with moderate surface coverage of capturing probe.

Effect of Nanostructured Microelectrode Morphology. The influence of the morphology of nanostructured microelectrodes on the performance of the assay was also investigated (Figure 5). Here, two different NME morphologies were generated using different electrodeposition potentials.[41] NME 1 exhibits a spiky and more dense morphology, while NME 2 possesses a less dense and more nanostructured morphology (Figure 5a). The concentration-dependent response in the presence of antibody was monitored, and we observed that NME 2 produced higher levels of sensitivity (Figure 5b) and gain (Figure 5c) by comparing its response to

DOI: 10.1021/acs.analchem.7b01595
Anal. Chem. 2017, 89, 9751−9757

two concentration of antibody, low (3 nM) and high (3 μM). The NME 2 structure is more highly nanostructured than that of NME 1, likely amplifying the steric blocking effects that the eSHHA assay reports on.

Enhancing eSHHA Sensitivity. The eSHHA takes advantage of the specificity of DNA−DNA hybridization to provide a specific signal correlated with the molecule of interest (e.g., protein or antibody). Therefore, the affinity of hybridization, which corresponds to the number of DNA base-pairs, has an important role in modulating the detection limit of the sensor. When employing macroelectrodes, utilizing longer DNA strands does not enhance detection sensitivity, despite of a higher hybridization affinity (Figure S2). This observation likely reflects the lower accessibility of DNA on macroelectrodes, due to elevated steric effects, electrostatic repulsion and orientation constraints. For a 16-base DNA capture strands immobilized on a macroelectrode, a 53% maximum gain reduction is achieved with a 10 nM detection limit with a model protein (streptavidin−biotin interaction, K_D = 40 fM[42]). However, in case of 32-base DNA strands on macroelectrodes, the maximum gain reduction is significantly reduced to 17% due to low accessibility of strands on the surface.

NMEs, in contrast, provide a nanostructured surface morphology that allow the immobilization of a higher density of longer capturing strands and also more efficient surface hybridization of longer singling strands (Figure 6). The 32-base capturing/signaling DNA strands, when used with NMEs, provide a gain reduction of 50% with low picomolar detection limit (10 pM for streptavidin, see Figure S3). A high density of 32-base strands on the surface have a $C_{50\%}$ of 20 nM upon hybridization to the 32-base complementary strands, which is 4-fold decrease in comparison to the 16-base strands with a $C_{50\%}$ of 80 nM (Figure 6a). By utilizing a moderate density of 32-base strands, the $C_{50\%}$ is reduced to 15 nM (Figure 6b). Finally, the maximum gain reduction achieved using streptavidin as a model analyte is 75% with a 5 min incubation (Figure 6c). This gain represents a 10-fold improvement over what has been reported so far for the detection of large proteins using eSHHA.[36] The improvement in gain at low signaling strand concentrations results in a significant improvement in detection limit for a protein analyte (Figure S3). Clearly, the use of NMEs rather than macroelectrodes improves the performance of the eSHHA assay.

CONCLUSION

The study reported here explored the factors that modulate a protein detection assay that leverages steric hindrance. In particular, the role of electrode morphology was shown to enhance the performance of the eSHHA approach. First, we showed that detection sensitivity is improved when nanostructured microelectrodes are used due to size-dependent hybridization rates and morphology-induced blocking effects on the surface. Accordingly, an improvement was realized for gain reduction using nanostructured microelectrodes compared to macroelectrodes. The response time was also improved as the consequence of size-dependent hybridization rate on nanostructured microelectrodes. Finally, we described the improvement of detection limits using longer DNA sequences on nanostructured microelectrodes. Thus, deploying nanostructured microelectrodes in this assay allows rapid time-to-answer, together with higher sensitivity and lower detection limits.

ASSOCIATED CONTENT

Supporting Information

The Supporting Information is available free of charge on the ACS Publications website at DOI: 10.1021/acs.analchem.7b01595.

Materials, chip fabrication, calculation, and report of capturing strand surface density, dose−response curves, and eSHHA response on the surface of macroelectrodes (PDF)

AUTHOR INFORMATION

Corresponding Author

*E-mail: shana.kelley@utoronto.ca.

ORCID

Alexis Vallée-Bélisle: 0000-0002-5009-7715

Shana O. Kelley: 0000-0003-3360-5359

Notes

The authors declare no competing financial interest.

ACKNOWLEDGMENTS

This work was supported by Genome Canada and the Ontario Genomics Institute (Grant OGI-077), the Province of Ontario through the Ministry of Research and Innovation (ORF-GAPP), and the Natural Sciences and Engineering Research Council of Canada (Discovery Grants S.O.K. and A.V.-B.).

REFERENCES

(1) Tavallaie, R.; De Almeida, S. R.; Gooding, J. J. *WIREs: Nanomed. Nanobiotechnol.* **2015**, *7*, 580.

(2) Ahmed, M. U.; Hossain, M. M.; Safavieh, M.; Wong, Y. L.; Abd Rahman, I.; Zourob, M.; Tamiya, E. *Crit. Rev. Biotechnol.* **2016**, *36*, 495.

(3) Lautner, G.; Gyurcsanyi, R. E. *Electroanalysis* **2014**, *26*, 1224.

(4) Sage, A. T.; Besant, J. D.; Lam, B.; Sargent, E. H.; Kelley, S. O. *Acc. Chem. Res.* **2014**, *47*, 2417.

(5) Kelley, S. O.; Mirkin, C. A.; Walt, D. R.; Ismagilov, R. F.; Toner, M.; Sargent, E. H. *Nat. Nanotechnol.* **2014**, *9*, 969.

(6) Drummond, T. G.; Hill, M. G.; Barton, J. K. *Nat. Biotechnol.* **2003**, *21*, 1192.

(7) Hu, J.; Yu, Y.; Brooks, J. C.; Godwin, L. A.; Somasundaram, S.; Torabinejad, F.; Kim, J.; Shannon, C.; Easley, C. J. *J. Am. Chem. Soc.* **2014**, *136*, 8467.

(8) Ricci, F.; Adornetto, G.; Palleschi, G. *Electrochim. Acta* **2012**, *84*, 74.

(9) Song, S.; Wang, L.; Li, J.; Zhao, J.; Fan, C. *TrAC, Trends Anal. Chem.* **2008**, *27*, 108.

(10) Vallée-Bélisle, A.; Plaxco, K. W. *Curr. Opin. Struct. Biol.* **2010**, *20*, 518.

(11) Clark, L. C., Jr.; Lyons, C. *Ann. N. Y. Acad. Sci.* **1962**, *102*, 29.

(12) Cass, A. E. G.; Davis, G.; Francis, G. D.; Hill, H. A. O.; Aston, W. J.; Higgins, I. J.; Plotkin, E. J.; Scott, D. L.; Turner, A. P. F. *Anal. Chem.* **1984**, *56*, 667.

(13) Barfidokht, A.; Gooding, J. J. *Electroanalysis* **2014**, *26*, 1182.

(14) Taufik, S.; Barfidokht, A.; Tanzirul Alam, M.; Jiang, C.; Parker, S. G.; Gooding, J. J. *J. Electroanal. Chem.* **2016**, *779*, 229.

(15) Jia, X.; Dong, S.; Wang, E. *Biosens. Bioelectron.* **2016**, *76*, 80.

(16) Luong, J. H.; Male, K. B.; Glennon, J. D. *Biotechnol. Adv.* **2008**, *26*, 492.

(17) Lapitan, L. D., Jr.; Guo, Y.; Zhou, D. *Analyst* **2015**, *140*, 3872.

(18) Xu, J. J.; Zhao, W. W.; Song, S.; Fan, C.; Chen, H. Y. *Chem. Soc. Rev.* **2014**, *43*, 1601.

(19) Zhou, W.; Gao, X.; Liu, D.; Chen, X. *Chem. Rev.* **2015**, *115*, 10575.

(20) Wang, Z.; Dai, Z. *Nanoscale* **2015**, *7*, 6420.

(21) Lord, H.; Kelley, S. O. *J. Mater. Chem.* **2009**, *19*, 3127.

DOI: 10.1021/acs.analchem.7b01595
Anal. Chem. 2017, 89, 9751−9757

(22) Wu, L.; Xiong, E.; Zhang, X.; Zhang, X.; Chen, J. *Nano Today* **2014**, *9*, 197−211.
(23) Hasanzadeh, M.; Shadjou, N.; de la Guardia, M. *TrAC, Trends Anal. Chem.* **2015**, *72*, 1.
(24) Rosi, N. L.; Mirkin, C. A. *Chem. Rev.* **2005**, *105*, 1547.
(25) Labib, M.; Sargent, E. H.; Kelley, S. O. *Chem. Rev.* **2016**, *116*, 9001.
(26) Zhou, Y. G.; Wan, Y.; Sage, A. T.; Poudineh, M.; Kelley, S. O. *Langmuir* **2014**, *30*, 14322.
(27) Soleymani, L.; Fang, Z.; Sargent, E. H.; Kelley, S. O. *Nat. Nanotechnol.* **2009**, *4*, 844.
(28) Besant, J. D.; Das, J.; Sargent, E. H.; Kelley, S. O. *ACS Nano* **2013**, *7*, 8183.
(29) Bin, X.; Sargent, E. H.; Kelley, S. O. *Anal. Chem.* **2010**, *82*, 5928.
(30) Bhimji, A.; Zaragoza, A. A.; Live, L. S.; Kelley, S. O. *Anal. Chem.* **2013**, *85*, 6813.
(31) Soleymani, L.; Fang, Z.; Lam, B.; Bin, X.; Vasilyeva, E.; Ross, A. J.; Sargent, E. H.; Kelley, S. O. *ACS Nano* **2011**, *5*, 3360.
(32) Soleymani, L.; Fang, Z.; Sun, X.; Yang, H.; Taft, B. J.; Sargent, E. H.; Kelley, S. O. *Angew. Chem., Int. Ed.* **2009**, *48*, 8457.
(33) Fang, Z.; Soleymani, L.; Pampalakis, G.; Yoshimoto, M.; Squire, J. A.; Sargent, E. H.; Kelley, S. O. *ACS Nano* **2009**, *3*, 3207.
(34) Sage, A. T.; Besant, J. D.; Mahmoudian, L.; Poudineh, M.; Bai, X.; Zamel, R.; Hsin, M.; Sargent, E. H.; Cypel, M.; Liu, M.; Keshavjee, S.; Kelley, S. O. *Sci. Adv.* **2015**, *1*, e1500417.
(35) Zhou, W. D.; Mahshid, S. S.; Wang, W. J.; Vallee-Belisle, A.; Zandstra, P. W.; Sargent, E. H.; Kelley, S. O. *ACS Sensors* **2017**, *2*, 495.
(36) Mahshid, S. S.; Camire, S.; Ricci, F.; Vallee-Belisle, A. *J. Am. Chem. Soc.* **2015**, *137*, 15596.
(37) Xiao, Y.; Lai, R. Y.; Plaxco, K. W. *Nat. Protoc.* **2007**, *2*, 2875.
(38) Gao, Y.; Wolf, L. K.; Georgiadis, R. M. *Nucleic Acids Res.* **2006**, *34*, 3370.
(39) Wetmur, J. G. *Crit. Rev. Biochem. Mol. Biol.* **1991**, *26*, 227.
(40) De Luna, P.; Mahshid, S. S.; Das, J.; Luan, B.; Sargent, E. H.; Kelley, S. O.; Zhou, R. *Nano Lett.* **2017**, *17*, 1289.
(41) Mahshid, S.; Mepham, A. H.; Mahshid, S. S.; Burgess, I. B.; Saberi Safaei, T.; Sargent, E. H.; Kelley, S. O. *J. Phys. Chem. C* **2016**, *120*, 21123.
(42) Holmberg, A.; Blomstergren, A.; Nord, O.; Lukacs, M.; Lundeberg, J.; Uhlen, M. *Electrophoresis* **2005**, *26*, 501.

DOI: 10.1021/acs.analchem.7b01595
Anal. Chem. 2017, 89, 9751−9757